A nonlocal elastica inspired by flexural tensegrity

A nonlocal elastica inspired by flexural tensegrity

Claudio BONI[a], Gianni ROYER-CARFAGNI[a,b,*]

[a] *Department of Engineering and Architecture, University of Parma, Parco Area delle Scienze 181/A, I-43100 Parma, Italy*

[b] *Construction Technologies Institute - Italian National Research Council (ITC-CNR), Via Lombardia 49, I-20098 San Giuliano Milanese, Milano, Italy*

Abstract

A nonlocal theory is presented for the bending in large deformations under applied loads of an initially straight rod. This has similarities with the classical Euler's elastica in the sense that the bending stiffness remains homogeneously constant, but it depends on an integral average of the entire curvature field. The discretized form of the equilibrium equations is identical to those governing the response of structural systems already called flexural tensegrity beams, composed of a chain of segments in unilateral contact, whose integrity under flexion is due to prestressing tendons and to the shape of the contact surfaces. An analytical method of solution is proposed modulo the calculation of elliptic integrals, which is compared in paradigmatic examples with the numerical approach, or with an approximation of the curvature field with shape functions. The comparison between the continuum theory and the discrete case of flexural tensegrity highlights the physical role of the constitutive parameters, paving the way for a tailored design of innovative devices and the modelling of complex biological structures, based on the capability of transforming the mechanical properties with very small changes at the level of the underlying micro-constituents.

Keywords:
elastica, nonlocal response, flexural tensegrity, analytical modelling, large

*Corresponding author
Email addresses: claudio.boni@unipr.it (Claudio BONI), gianni.royer@unipr.it (Gianni ROYER-CARFAGNI)

deflections.

1. Introduction

In *Additamentum I* "*De curvis Elasticis*" to his famous treatise of 1744, Euler (1744)[1] celebrates Daniel Bernouilli for having suggested that the *universam vim* of a curved elastic lamina could be compacted in one single formula called *vim potentialem*, and such an expression shall be minimal for the *curva Elastica*. Developing Bernoulli's idea, Euler showed that the differential equation determining the curve, or *elastica*, in which a thin rod, straight and prismatic in the unstressed state, is held by forces and couples when bent in a principal plane - so that the central line becomes a plane curve - could be found by making a minimum the integral of the square of the curvature taken along the rod (Thomson and Tait, 1883; Love, 1944).

Euler's elastica is a simple model that it is often advocated as the paradigm for compliant structures. It applies to biology, e.g., to conveniently describe the deformation of collagen fibers (Diamant et al., 1972), or to study the locomotion provided by flexible flagella to bacteria (Tournus et al., 2015). The model is widely used in mechanical engineering and soft robotics (Wilson and Snyder, 1988; Yamada et al., 2007), as well as for biomedical tools (Chen and Li, 2007). "Unusual" applications can be found in a hot-cutting robot for the fabrication of formworks for concrete shell structures (Søndergaard et al., 2016), in devices for timber transportation along rivers (Newman, 1975) and in cattle-catching tools like the *lasso* (Brun et al., 2014). From a more fundamental point of view, flexible and inextensible elastic rods have been used by Bigoni and co-workers as the basic structural models to describe phenomena and applications yet to be fully appreciated. An elastic rod constrained within a frictionless sliding sleeve provides the simplest illustration of the role played by configurational, or Eshelby-like forces, on the statics (Bosi et al., 2015a) and dynamics (Armanini et al., 2019) of one-dimensional structures. This finding has suggested novel ingenious devices, like a deformable arm scale (Bosi et al., 2014), as an alternative to the traditional rigid arm balance. The elastica can be used to describe the effects of surface tension in

[1] Reference (Euler, 1744) is the original Latin version of Euler's work, also available in (Euler, 1952). An English translation with comments can be found in (Oldfather et al., 1933).

fluids, such as self-encapsulation or dripping (Bosi et al., 2015b), with potential applications in electro-magnetic circuits. Drawing inspiration from antique weapons, the optimization of a flexible rod as a catapult (Armanini et al., 2017) suggests the design for innovative robotic limbs.

All the aforementioned applications make use of the classical theory of the elastica. This has been geometrically linearized, treated with imperfections, analyzed for bifurcation points, relaxed to include extensibility but, fundamentally, the original stored-energy function has been maintained in its dependence on the square of the curvature. Non-quadratic energies have sometimes been used to describe nonlinear constitutive responses between bending moment and local curvatures. Strain energy functionals derived from non-convex potentials in the curvature field (Fosdick and James, 1981) predict, as absolute minimizers, discontinuous curvatures of the central line even under pure bending (prescribed terminal slope-angles or couples), which recall the coexistent phases in stressed solid mixtures. Non-convex strain-energy densities with linear growth at infinity (oblique asymptotes), providing moment-curvature relationships with strain-softening branches and horizontal asymptotes, can induce the localization of bending strains as in a plastic hinge (Royer-Carfagni, 2001). Under the Euler-Bernoulli hypothesis that cross sections remain plane after the deformation, laws of this type were obtained by Royer-Carfagni and Buratti (2007) for elastic-plastic materials exhibiting a transition from the upper to the lower yield point, commonly experienced in strain-driven tests on low-carbon-steel bars (Froli and Royer-Carfagni, 2000), which is equivalent to a strain-softening branch.

Nonlocal theories for inflexed rods have been inspired by the seminal work by Eringen (1983). Nonlocal *differential* (high-order gradient) elastic constitutive relations have been successfully used to describe the equilibrium states and vibration modes of carbon nanotubes (Thai, 2012). The differential form is often considered as an approximation of the complete *integral* formulation, in which the bending depends upon the convolution between the elastic curvature and an averaging kernel, usually with compact support or with a fast decay at infinity. For models of this kind, an issue of paramount importance is the compatibility between the boundary conditions consequent to the nonlocal constitutive law and the equilibrium conditions that the bending field has to satify (Romano et al., 2017). In order to overcome possible emerging paradoxes, stress-driven nonlocal theories have been also proposed by Romano and Barretta (2017), where it is the elastic curvature field that depends upon convolution between the bending field and an averaging kernel.

Here, a particular nonlocal constitutive law, never considered before to the best of our knowledge, is proposed and analyzed in detail. The bending moment at each cross section depends linearly upon the curvature, but the bending stiffness, although remaining homogenously constant in the whole rod, is affected by the whole curvature field. This is fundamentally different from all the cases mentioned before, in which the bending moment at each point of the centroidal line is at most a nonlinear function of the local curvature and its gradients, or depends upon the values of the curvature field in a neighborhood of the point.

The motivation for such a peculiar response stems from the *flexural tensegrity* concept, recently proposed by Boni et al. (2020) while developing the embryonal idea of Beatini and Royer-Carfagni (2013). The term "tensegrity" was coined by Buckminster Füller to indicate a prestress-stable structural system whose *integrity* is due to *tensile* members, usually cables, pre-tensioned by matching a few floating compression struts (Sadao, 1996). "Flexural tensegrity" indicates a condition in which the *integrity* under *flexure* of a mobile chain, composed by segments in unilateral contact, is assured by tendons that press the segments together. Besides the cable tension, the constitutive response depends upon the shape of the contact surfaces between consecutive segments, identified by the corresponding pitch lines and constructed by Boni et al. (2020) with a double couple of conjugate profiles. In this system, the internal constraint between any two consecutive segments is equivalent to a spring hinge. The response is nonlocal in type, because the cable elongation and consequently its axial force, which governs the effective stiffness of the spring hinges, depends upon the rotations of *all* the segments. The continuum counterpart of this segmental construction is the nonlocal elastica presented in this article.

With reference to the paradigmatic case-study of a simply supported rod under the most general loading conditions, the continuum nonlocal theory is presented in Section 2. After detailing its derivation from flexural tensegrity, it is shown how the equilibrium states of the rod can be determined analytically modulo the calculation of elliptic integrals, as in the case of Euler's elastica. Indeed, the analysis of exemplificative cases, pursued in Section 3 either with the analytical approach or with a direct numerical calculation, demonstrates the strict correlation, but with fundamental differences, of the most well-known model by Euler with the proposed nonlocal rod. This represents an innovative flexible structure which, while respecting the orthodoxy of the classical elastica, can be tuned for a tailored design in a wide range of

applications.

2. The model

After presenting the analytical theory of the nonlocal elastica, its derivation from flexural integrity is indicated, also with reference to a physical model. The nonlocal effect is discussed and methods of solution of the equilibrium equations are proposed.

2.1. The elastica with nonlocal bending stiffness

Consider the problem of determining the equilibrium states of a thin rod, straight in its undistorted reference configuration, which is bent in a principal plane so that the centerline becomes a plane curve. The rod, of length L, is simply supported at the ends as represented in Figure 1(a), and we take a system of fixed axes x, y, with x coinciding with the centerline in the unstressed state. The rod bends, as schematically indicated in Figure 1(b), under the action of a distributed load $p(s)$, being $s \in [0, L]$ the curvilinear abscissa identifying points on the centerline, two opposite horizontal end-forces F, positive if they induce compression, and two couples M_l and M_r, applied at the left- and right-hand-side ends, respectively. Let $u(s)$ and $v(s)$ denote the components on x, y of the displacement of the point at s, positive if opposite to the orientation of the axes, and let $\varphi(s)$ represent the angle here formed between the tangent to the deformed centerline and the x axis, considered positive if it corresponds to a clockwise rotation. Hence, the curvature at s is given by $\chi = -\varphi'(s)$.

Assume that the elastic strain energy $\mathcal{U}$ is of the form

$$\mathcal{U} = \mathcal{U}[\varphi] = \frac{1}{2} K_L \int_0^L (-\varphi'(s))^2 \, ds + \frac{l^2}{4L} K_{NL} \left[\int_0^L (-\varphi'(s))^2 \, ds \right]^2 , \quad (2.1)$$

where K_L and K_{NL} are constants with dimension $[ML^3T^{-2}]$ and l denotes an intrinsic length scale, whose physical role will be detailed in Section 2.2. In the case in which $K_{NL} = 0$, the model falls in the category of classical Euler's elastica. With respect to this case, the term associated with K_{NL} provides a nonlocal effect and additional bending stiffness.

The work $\mathcal{W}$ of the external loads of Figure 1, written as a function of $\varphi(s)$, takes the form

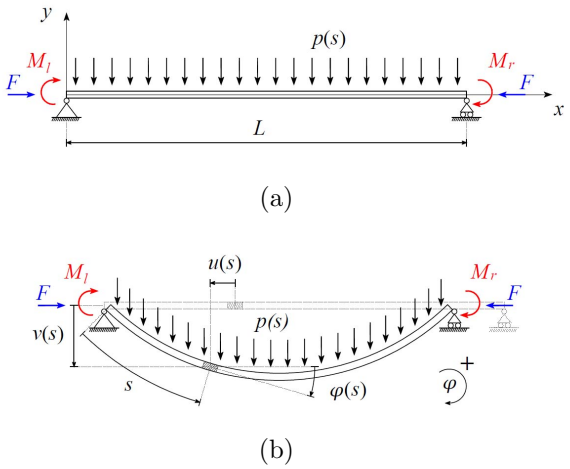

Figure 1: Model problem of a simply-supported nonlocal rod. (a) Reference undeformed configuration and (b) deformed state under the action of the applied forces and couples.

$$\mathcal{W} = \mathcal{W}[\varphi] = \int_0^L p(s) \left[\int_0^s \sin\left(\varphi(\bar{s})\right) d\bar{s} \right] ds + \\ + F \int_0^L \left[1 - \cos\left(\varphi(s)\right)\right] ds + M_l\, \varphi(0) + M_r\, \varphi(L)\,. \tag{2.2}$$

In addition, the kinematic compatibility with the roller constraint at $s = L$ implies that

$$\mathcal{G} = \mathcal{G}[\varphi] = \int_0^L \sin(\varphi(s)) ds = 0\,. \tag{2.3}$$

The equilibrium states correspond to the solution of the minimization problem $\mathcal{U}[\varphi] - \mathcal{W}[\varphi] = \min$, under the constraint $\mathcal{G}[\varphi] = 0$. Introduced the augmented functional $\mathcal{H}[\varphi] = \mathcal{U}[\varphi] - \mathcal{W}[\varphi] + \lambda \mathcal{G}[\varphi]$, where λ is the Lagrange multiplier, for a variation $\varphi + \delta\varphi$, the first variation of $\mathcal{H}[\varphi]$ reads

$$\mathcal{H}[\varphi|\delta\varphi] = \left[K_L + K_{NL}\frac{l^2}{L}\int_0^L (\varphi'(s))^2 ds\right]\left[\int_0^L \varphi'(s)\delta\varphi'(s)ds\right] + \\ - \int_0^L p(s)\left[\int_0^s \cos\left(\varphi(\bar{s})\right)\delta\varphi(\bar{s})d\bar{s}\right]ds - M_l\,\delta\varphi(0) - M_r\,\delta\varphi(L) + \\ - F\int_0^L \sin\left(\varphi(s)\right)\delta\varphi(s)ds + \lambda\int_0^L \cos\left(\varphi(s)\right)\delta\varphi(s)ds\,. \tag{2.4}$$

Considering a variation $\delta\varphi$ with unit mass and centered at s^* with compact support in the interval $[s^* - \Delta s/2,\, s^* + \Delta s/2]$, one finds

$$\int_0^s \cos\left(\varphi(\bar{s})\right)\delta\varphi(\bar{s})d\bar{s} = \int_{s^*-\frac{\Delta s}{2}}^s \cos\left(\varphi(\bar{s})\right)\delta\varphi(\bar{s})d\bar{s}\,, \tag{2.5}$$

for $s \in [s^* - \Delta s/2\,,\, L]$, and by letting $\Delta s \to 0$, the variation itself becomes a Dirac Delta distribution centered at $s = s^*$. After integration by parts, one obtains the field equations

$$\left[K_L + K_{NL}\frac{l^2}{L}\int_0^L (\varphi'(s))^2 ds\right]\varphi''(s^*) + F\sin(\varphi(s^*)) + \\ + \left[\int_{s^*}^L p(s)ds - \lambda\right]\cos(\varphi(s^*)) = 0\,, \\ \int_0^L \sin(\varphi(s))ds = 0\,, \tag{2.6}$$

with integral conditions at the boundary

$$\left[K_L + K_{NL}\frac{l^2}{L}\int_0^L (\varphi'(s))^2 ds\right]\varphi'(0) = -M_l\,, \\ \left[K_L + K_{NL}\frac{l^2}{L}\int_0^L (\varphi'(s))^2 ds\right]\varphi'(L) = M_r\,. \tag{2.7}$$

Observe that boundary conditions of this kind do not present the inconvenience discussed by Romano et al. (2017) because the nonlocal effect is not obtained as a convolution between the elastic curvature and an averaging

kernel, which may provide spurious results when the convolution is evaluated in a neighborhood of the ends of the rod. Here, the flexural stiffness is *homogeneously* increased in the whole rod, according the quadratic mean of the curvature. The classical equations of Euler's (local) elastica are obtained when $K_{NL} = 0$ and, in this limit, the flexural stiffness is K_L.

It is worth mentioning that an interesting result in the classical problem of the elastica, in the case in which no forces or couples are applied to the rod except at the ends, is that there is a conserved quantity, equivalent to the energy-integral of the equations of motion in Kirchhoff's kinetic analogue, expressed by eq. (3) of art. 260 in the treatise by Love (1944). To be more explicit, consider, for example, the simplest case of a cantilever $s \in [0, L]$, initially straight, clamped at $s = 0$ and loaded by the axial force F at $s = L$. In this case, the governing equation can be derived from $(2.6)_1$ with $K_{NL} = 0$, $p(s) = 0$, $\lambda = 0$, and reads $K_L\varphi'' + F \sin\varphi = 0$. In the kinetic analogue (Love, 1944), substituting differentiation with respect to the variable s with the time derivative, this equation applies to the varying angle $\varphi(t)$ that a rigid pendulum turning around a fixed horizontal axis, with a hanging mass proportional to F, forms with the vertical in the time interval $t \in [0, L]$.

However, in the presented nonlocal theory, the bending stiffness is not constant, but depends on the squared Lebesgue norm of the curvature, so that the classic argument does not hold. The *periodicity in space* of the curves representing a family of elastica solutions is lost in the nonlocal case, because the bending stiffness depends upon the length of the rod that is considered. Consequently, also the *periodicity in time* in the envisaged kinetic analogue would fail. This is why it is difficult, at least at this stage, to establish a correspondence between the well-known phase space for the classic elastica under terminal loadings and the phase space associated with $(2.6)_1$. A characterization of this type will be the subject of further work.

2.2. Motivation from flexural tensegrity

A real beam-like structure with the aforementioned constitutive properties should have the following characteristics: *i*) its cross sections are constant and symmetric with respect to the bending plane and the centroidal axis orthogonal to that; *ii*) it is constituted by large number of very thin *segments* in unilateral contact; *iii*) it is prestressed by tendons (cables) whose effect is equipollent to that of one tendon located in the geometric centroid of the cross section; *iv*) the tendons are unbonded and efficiently lubricated within the sheaths, so that they have permanent freedom of longitudinal movement

relative to the segments; *v*) as a consequence of bending, internal equilibrium at each cross section is provided by the tensile force in the cable and the resultant of the contact stress between the adjacent segments; *vi*) the lever arm between the aforementioned forces is a linear function of the local curvature. The most important hypothesis is the last one, which can be verified only in particular conditions.

The bending deformation is described by the function $\varphi(s)$, indicated in Figure 1(b). At each cross section s, let N and $R(s)$ respectively denote the tensile force in the cable, independent of s, and the resultant of contact stresses in the adjacent segments. Let $a(s)$ represent the lever arm of the internal forces, i.e., the distance between N and the point of application of $R(s)$. According to the hypothesis *vi*), set $a(s) = -l^2\varphi'(s)$, where l is the intrinsic length scale introduced in Section 2.1, which now acquires a physical interpretation from the geometry of the contact surfaces.

The strain energy $\mathcal{U}$ is the sum of the part $\mathcal{U}_{\text{cable}}$ stored in the cable, consequent to its prestress and additional elongation under bending, and the part $\mathcal{U}_{\text{matrix}}$ in the material matrix forming the segments, due to the elastic deformation under contact. If Λ denotes the elongation of the cable due to bending, then N is a function of Λ. Further supposing that $\mathcal{U}_{\text{matrix}} \ll \mathcal{U}_{\text{cable}}$, as it is the case when the matrix is so stiff to be considered rigid with respect to the cable, for an infinitesimal increase of length $d\Lambda$ one can write

$$d\mathcal{U} \simeq d\mathcal{U}_{\text{cable}} = N(\Lambda)\, d\Lambda\,. \tag{2.8}$$

Hence, for an infinitesimal increase of the curvature field $d\chi = -d\varphi'(s)$, one can write

$$\begin{aligned} d\mathcal{U} &= \int_0^L N(\Lambda)a(s)\,(-d\varphi'(s))\,ds = N(\Lambda)\,l^2 \int_0^L (\varphi'(s)d\varphi'(s))\,ds = \\ &= N(\Lambda)\,l^2 \int_0^L \frac{1}{2}\,d\,(\varphi'(s))^2\,ds = N(\Lambda)\,d\left[\int_0^L \frac{l^2}{2}\,(\varphi'(s))^2\,ds\right]\,. \end{aligned} \tag{2.9}$$

Equation (2.9) coincides with (2.8) provided that the elongation of the cable satisfies

$$d\Lambda = d\left[\int_0^L \frac{l^2}{2}\,(\varphi'(s))^2\,ds\right] \quad \Rightarrow \quad \Lambda = \frac{l^2}{2}\int_0^L (-\varphi'(s))^2 ds\,. \tag{2.10}$$

Denote now with E_c, A_c and L_0 the Young's modulus, cross-sectional area and undistorted length of the cable, respectively. Calling Λ_0 its elongation in the undistorted state, so that the initial prestress is $N_0 = E_c A_c \Lambda_0 / L_0$, the elastic energy takes the form

$$\mathcal{U} = \int_0^{\Lambda} \frac{E_c A c}{L_0} (\Lambda_0 + \bar{\Lambda})\, d\bar{\Lambda} = N_0 \Lambda + \frac{E_c A_c}{2 L_0} \Lambda^2 \,, \tag{2.11}$$

Hence, using (2.10), one obtains

$$\mathcal{U} = N_0 \frac{l^2}{2} \int_0^L (-\varphi'(s))^2 ds + \frac{E_c A_c l^4}{8 L_0} \left[\int_0^L (-\varphi'(s))^2 ds \right]^2 , \tag{2.12}$$

It is immediate to recognize that (2.12) is identical to (2.1), with

$$K_L = N_0 l^2 \,, \quad K_{NL} = \frac{E_c A_c l^2}{2} \frac{L}{L_0} \,. \tag{2.13}$$

The *flexural tensegrity* segmental beam proposed by Boni et al. (2020) fulfills, in the continuum limit, the aforementioned basic hypotheses, in particular the dependence of the lever arm $a(s)$ on the curvature $-\varphi'(s)$ and the dependence of the cable elongation Λ on the squared Lebesgue norm of the curvature, as per (2.10). This is formed by rigid segments, of finite length, held together by a centroidal prestressing tendon (cable), anchored at the beam ends, as schematically represented in Figure 2. The segmental beam is straight in the reference configuration of Figure 2(a) and bends under the action of external loads as indicated in Figure 2(b). Each segment is pierced and hosts a sheath where the cable can slide with negligible friction. More important, the contact surfaces between any two consecutive segments are properly shaped so that, under bending, the facing surfaces are designed to roll with no sliding along particular pitch lines. As a consequence of a relative rotation $\Delta\varphi_i$ of the segments at the $i-$th contact joint, the cable elongates of Λ_i, as shown in Figure 2(c). Remarkably, the distance between the pitch point and the portion of the cable that becomes exposed during bending, is the lever arm a_i of the tension force N in the cable, as per Figure 2(c).

In order to achieve a linear relationship between a_i and $\Delta\varphi_i = \varphi_i - \varphi_{i+1}$, circular pitch lines may be chosen. Arcs of circle of radius R provide the law $a_i = R\Delta\varphi_i/2$ only approximatively, but the error is less than 1.0% when

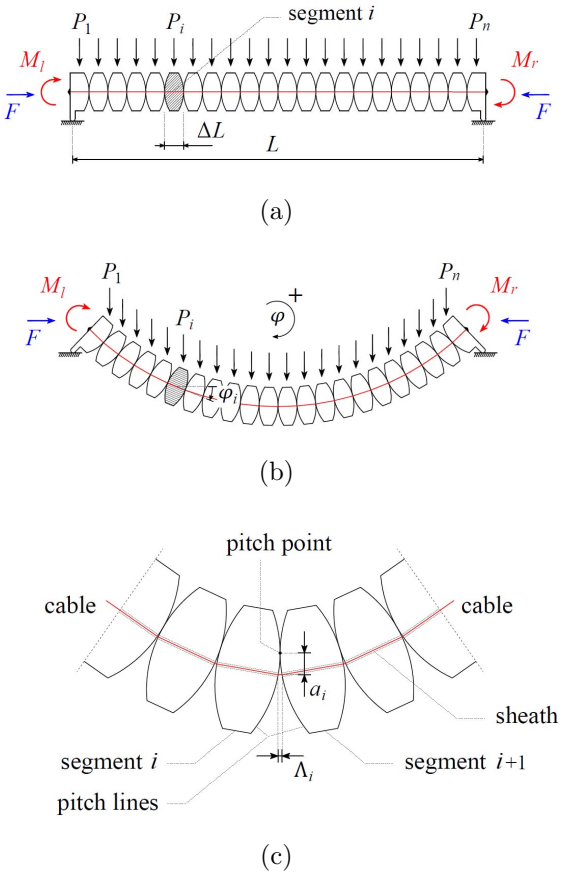

Figure 2: Schematic representation of the simply-supported flexural-tensegrity beam. (a) Reference undeformed configuration; (b) deformed state; (c) detail of the $i-$th contact joint, after the relative rotation of the beam segments, with indication of the cable elongation Λ_i and the lever arm a_i of the tensile force N with respect to the pitch point.

$\Delta\varphi_i = 30°$. With arcs of ellipse, as shown by Boni et al. (2020), a better approximation can be obtained, but the difference is insignificant.

The discretized version of the equilibrium equations (2.6) for the nonlocal elastica provides the basis for their numerical solution with the finite difference method, but it also corresponds to the equations for the tensegrity beam of Figure 2. Denoting with ΔL the discretization step, coinciding with the length of the segment in the flexural tensegrity counterpart, derivatives are substituted by difference quotients and integrals by summations. Of course, the distributed load $p(s)$ needs to be approximated by a set of forces P_i applied at the segment centroid, such that $p(s_i - \Delta L/2) = P_i/\Delta L$, being $s_i = i\,\Delta L$ the curvilinear abscissa at the $i-$th node. The continuous model is obtained as the length of the segments tends to zero and their number to infinity. In particular, one can set

$$-\varphi'(s) \simeq \frac{\varphi_i - \varphi_{i+1}}{\Delta L}\,, \quad \varphi''(s) \simeq \frac{\varphi_{i+1} - 2\varphi_i + \varphi_{i-1}}{\Delta L^2}\,, \tag{2.14}$$

where φ_i is the absolute rotation of the discretization segment i for $i = 1 \dots n$, with n the number of subdivisions.

It is interesting to observe that, for circular pitch lines of radius R, the counterpart in the discrete model of the intrinsic length-scale l of (2.1) is of the form $l^2 = R\,\Delta L/2$. Hence, in order to obtain a finite limit for l^2 in the continuum model, one has to assume that $\lim_{\Delta L\to 0} R = +\infty$; this means that for segments of infinitesimal length, the pitch lines at the contact joints are almost straight.

The discretized form of equations (2.6) read

$$\begin{aligned} &N\,\frac{a_i - a_{i-1}}{\Delta L} + \left[\lambda + \frac{P_i}{2} - \sum_{j=i}^{n} P_j\right]\,\cos(\varphi_i) + \\ &\qquad - F\,\sin(\varphi_i) - \mathbb{I}_1(i)\frac{M_l}{\Delta L} - \mathbb{I}_n(i)\frac{M_r}{\Delta L} = 0\,, \\ &\sum_{j=1}^{n} \Delta L\,\sin(\varphi_j) = 0\,, \quad i = 1 \dots n\,, \end{aligned} \tag{2.15}$$

where $N = N_0 + \Delta N = N_0 + E_c A_c \Lambda / L_0$ is the tensile force in the cable, $a_i = l^2 \Delta\varphi_i$ is the internal lever arm, and $\mathbb{I}_i(j)$ is the indicator function, which equals 1 when $i = j$, zero otherwise. The cable stretches, at each node i, of

the quantity $\Lambda_i = 0.5\, l^2 \Delta\varphi_i^2 / \Delta L$, so that the global elongation is defined by $\Lambda = \sum_{i=1}^{n-1} \Lambda_i$, being n the number of subdivisions. Equations (2.15) are the same found by Boni et al. (2020) when analyzing flexural tensegrity segmental beams, even if now for a more general loading condition, but here they have been obtained from the discretization of the continuum model presented in Section 2.1.

In order to compare the theoretical curves obtained from the nonlocal continuum theory with the physical model of flexural tensegrity segmental beams, the prototype displayed in Figure 3 has been manufactured in the same way indicated by Boni et al. (2020). The prototype, 3D-printed in polyethylene terephthalate, is composed of 32 segments of length 17.3 mm (total length of 553.6 mm), for which $l^2 = 100.6\,\mathrm{mm}^2$. The prestressing cable is a polyamide 6.6 wire of diameter 0.8 mm, with two springs of constant $\kappa = 2.8\,\mathrm{N/mm}$ added in series, as shown in Figure 3(a), so that $K_{NL} \simeq 21375\,\mathrm{Nmm}^2$. The deformation under self weight is represented in Figure 3(b). The relative displacement of any two consecutive segments is a rolling motion along the design circular pitch lines, which has been obtained in the practice by shaping the contact surfaces with a double couple of conjugate profiles, according to the layered construction detailed by Boni et al. (2020).

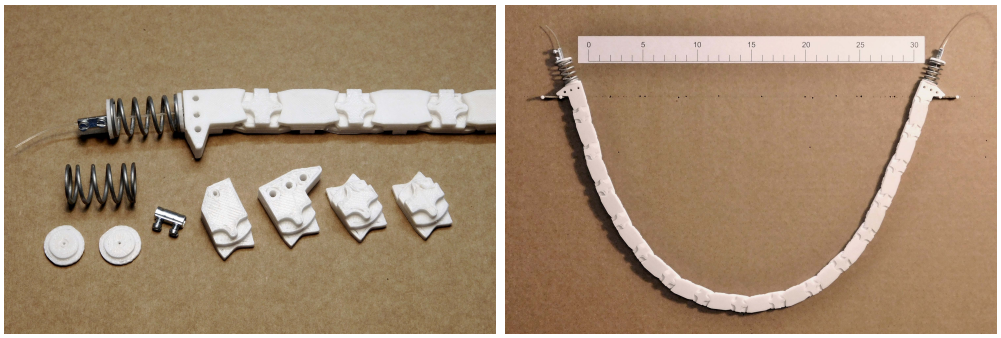

(a) (b)

Figure 3: Flexural tensegrity segmental beam: (a) constituting segments for which the theoretical pitch lines at the contact surfaces are obtained with a double couple of conjugate profiles; (b) deflection of the prototype under self-weight.

2.3. Nonlocal effect and the semi-analytical method of solution

The difference with classical Euler's elastica is represented by the nonlocal term in (2.1). In the physical segmental model of Figure 2, this is consequent to the fact that the tendon (cable) is not bonded to the material matrix, so that its elongation is affected by the whole curvature field. There is a remarkable difference between the present model and a nonlocal elastica for which the bending is governed by the convolution between the curvature field and an average kernel with compact support. In the second case, the nonlocal effect is localized in a neighborhood of the cross section, whereas in our case the bending stiffness is *homogeneously* and *uniformly* modified along the entire length of the rod.

Indeed, it is clear from (2.6) and (2.7) that the inflexion of the nonlocal elastica is identical to that of a classical Euler's elastica with *effective bending stiffness* K^*, of the form

$$K^* = K_L + K_{NL}\frac{l^2}{L}\int_0^L (\varphi'(s))^2 ds\,. \tag{2.16}$$

This observation suggests that, if the solution of the Euler's elastica is known as a function of its bending stiffness, then the solution can be found also for the nonlocal case.

To illustrate, consider the curve attained under applied loads by a classical Euler's elastica of bending stiffness K^*, and let $\varphi^*(s)$ represent the angle of rotation of its tangent at s with respect to the undeformed straight configuration. Then, calculate the function

$$f(K^*) = \int_0^L \left[(\varphi^*(s))'\right]^2 ds\,. \tag{2.17}$$

In order to solve the nonlocal case, it is sufficient to observe from (2.16) that

$$K^* = K_L + K_{NL}\frac{l^2}{L}f(K^*) \quad \Rightarrow \quad \frac{(K^* - K_L)L}{l^2 K_{NL}} = f(K^*)\,. \tag{2.18}$$

Consequently, the *actual* curve taken by the *nonlocal elastica* is the one corresponding to the deformation of that *Euler's elastica*, whose bending stiffness is found from the intercept of the graph of the function $\eta = f(K^*)$ with the line $\eta = (K^* - K_L)L/(l^2 K_{NL})$.

In general, the solution of Euler's elastica prescribes the calculation of elliptic integrals. In the past it was necessary to estimate them with tables (Jahnke and Emde, 1945), but nowadays they can be evaluated numerically using commercial softwares. Since the method described above is based on a analytical formulation, but eventually a numerical approach will be used to solve the elliptic integrals, the solution found in this way will be referred to as the *semi-analytical solution*.

The method is firstly clarified in an elementary example for which the field $\varphi^*(s)$ can be found in closed form, i.e., the case in which the rod of Figure 1(a) is bent by the two couples $M_l = M$ and $M_r = -M$. The deformed shape is an arc of a circle and the rotation field takes the form

$$\varphi^*(s) = \frac{M}{2K^*}(L - 2s)\,. \tag{2.19}$$

From (2.17) and (2.18), the actual stiffness K^* coincides with the real root of the cubic equation

$$\frac{(K^* - K_L)L}{l^2 K_{NL}} = f(K^*) = \frac{M^2 L}{(K^*)^2}\,. \tag{2.20}$$

For the case $M = 50\,\mathrm{Nm}$, $K_L = 10\,\mathrm{Nm}^2$, $K_{NL} = 150\,\mathrm{Nm}^2$, $l^2 = 0.1\,\mathrm{m}^2$ and $L = 3\,\mathrm{m}$, its graphical solution, providing the value $K^* = 37.16\,\mathrm{Nm}^2$, is shown in Figure 4(a).

The cases in which a concentrated load P is applied at midspan or, alternatively, the rod is axially compressed by two end-forces F, can be similarly treated. The starting point is again the solution of Euler's elastica with arbitrary bending stiffness K^*. Using symmetry, one can equivalently consider a cantilever of length $L/2$ loaded at the free end by a force $P/2$ orthogonal to the undeformed centerline or by an axial force F. The first case was solved by Bisshopp and Drucker (1945), while the second one has been reported in classical books (Love, 1944; Thomson and Tait, 1883) and, more recently, by Bigoni (2012). Let φ_0 represent the rotation at the tip of the cantilever, to be determined. Define the quantities $\mathcal{P}_0$, μ and ϑ_1 as

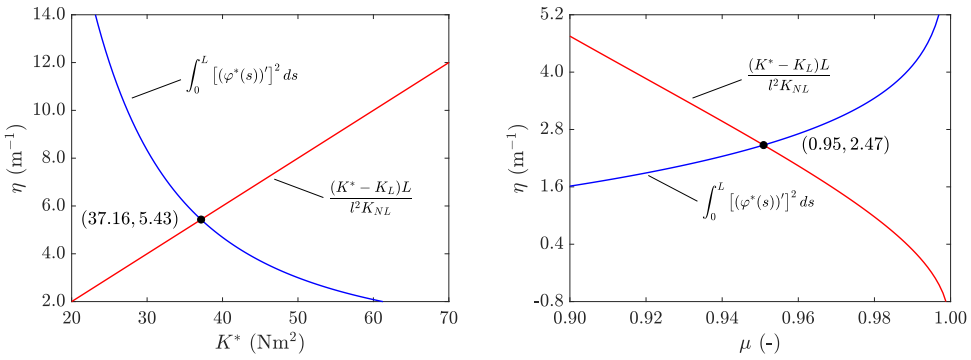

Figure 4: Graphs of the functions $\eta = \int_0^L \left[(\varphi^*(s))'\right]^2 ds$ and $\eta = (K^* - K_L)L/(l^2 K_{NL})$ for a simply supported rod subjected to (a) pure bending under end-couples $M_l = -M_r = M$ (plotted as a function of the effective stiffness K^*) and (b) a concentrated force P at midspan (plotted as a function of the elliptic parameter μ). Case $M = 50\,\mathrm{Nm}$, $P = 80\,\mathrm{N}$, $K_L = 10\,\mathrm{Nm}^2$, $K_{NL} = 150\,\mathrm{Nm}^2$, $l^2 = 0.1\,\mathrm{m}^2$ and $L = 3\,\mathrm{m}$.

$$\left.\begin{aligned} &\mathcal{P}_0 = P/2 \\ &\mu = [1 + \sin(\varphi_0)]/2 \\ &\vartheta_1 = \arcsin(1/\sqrt{2\mu}) \end{aligned}\right\} \text{ for midspan concentrated load } P\,,$$

$$\left.\begin{aligned} &\mathcal{P}_0 = F \\ &\mu = [1 - \cos(\varphi_0)]/2 \\ &\vartheta_1 = 0 \end{aligned}\right\} \text{ for compression axial load } F\,.$$

Then, for any value of the bending stiffness K^*, the value $\mu = \mu^*$ that solves the problem is found from the equation

$$K^* = \frac{\mathcal{P}_0 L^2}{4\left[\mathcal{F}(\frac{\pi}{2}, \mu) - \mathcal{F}(\vartheta_1, \mu)\right]^2}\,, \tag{2.21}$$

where

$$\mathcal{F}(\phi, \mu) = \int_0^\phi \frac{d\theta}{\sqrt{1 - \mu \sin^2(\theta)}}\,, \tag{2.22}$$

represents the incomplete elliptic integral of the first kind. The actual value ${\varphi_0}^*$ can be determined once μ^* is known. The corresponding curvature field $\chi^* = -(\varphi^*(s))'$ admits the representation

$$(\varphi^*(s))' = \begin{cases} \sqrt{\dfrac{P}{K^*}}\,[\sin({\varphi_0}^*) - \sin(\varphi^*(s))]^{\frac{1}{2}} & \text{for midspan load } P\,, \\ \sqrt{\dfrac{2F}{K^*}}\,[\cos(\varphi^*(s)) - \cos({\varphi_0}^*)]^{\frac{1}{2}} & \text{for axial load } F\,. \end{cases} \tag{2.23}$$

Hence, one can find the intercept of $\eta = f(K^*)$ with the line $\eta = (K^* - K_L)L/(l^2 K_{NL})$. It should be observed that (2.23) can be conveniently expressed through elliptic integrals as a function of the only variable μ, so that the elliptic parameter μ can be used to restate the condition (2.18). After some calculations, one finds that the solution $\mu = \mu^*$ for the *nonlocal elastica* is the solution of the equation

$$\begin{aligned} &\eta = f\left(K^*(\mu)\right) = \int_0^L \left(\varphi'(s,\mu)\right)^2 ds = \\ &= \frac{16\,\mu}{L}\left[\mathcal{F}(\tfrac{\pi}{2},\mu) - \mathcal{F}(\vartheta_1,\mu)\right]\left[\mathcal{F}(\tfrac{\pi}{2},\mu) - \mathcal{F}(\vartheta_1,\mu) - \mathcal{D}(\tfrac{\pi}{2},\mu) + \mathcal{D}(\vartheta_1,\mu)\right] = \\ &= \frac{\mathcal{P}_0 L^3}{4\,l^2 K_{NL}[\mathcal{F}(\frac{\pi}{2},\mu) - \mathcal{F}(\vartheta_1,\mu)]^2} - \frac{K_L L}{l^2 K_{NL}} = \frac{[K^*(\mu) - K_L]\,L}{l^2 K_{NL}}\,, \end{aligned} \tag{2.24}$$

where $\mathcal{D}(\phi,\mu)$ is a combination of the incomplete elliptic integral of the first kind $\mathcal{F}(\phi,\mu)$ and the incomplete elliptic integral of the second kind $\mathcal{E}(\phi,\mu)$, which take the form

$$\mathcal{E}(\phi,\mu) = \int_0^\phi \sqrt{1 - \mu\sin^2(\theta)}\,d\theta\,, \tag{2.25}$$

$$\mathcal{D}(\phi,\mu) = \frac{\mathcal{F}(\phi,\mu) - \mathcal{E}(\phi,\mu)}{\mu} = \int_0^\phi \frac{\sin^2(\theta)d\theta}{\sqrt{1 - \mu\sin^2(\theta)}}\,. \tag{2.26}$$

For the same material parameters considered for the case of Figure 4(a), Figure 4(b) shows the graphical solution of (2.18) in terms of the elliptic parameter μ for the case of a midspan load $P = 80\,\mathrm{N}$. In this way, one obtains the value $\mu^* = 0.95$ and, from this, $K^* = 22.35\,\mathrm{Nm}^2$ and ${\varphi_0}^* = 1.12\,\mathrm{rad}$.

The semi-analytical approach could also be used when the rod of Figure 1(a) is bent by a load $p(s)$ distributed along its length. When $p(s)$ follows a constant, triangular or sinusoidal law, the deformation of the Euler's elastica can be found (Mingari Scarpello and Ritelli, 2011) in terms of Lauricella ${F_D}^{(3)}$ hypergeometric functions (Lauricella, 1893). However the calculations become very complicated, so that a simple numerical method based on finite differences, as detailed in Section 2.4, turns out to be much more convenient.

To conclude this section, it may be useful to estimate the "strength" of the nonlocal effect with reference to the physical *flexural tensegrity* model of Section 2.2. Using (2.13), the effective stiffness (2.16) becomes

$$K^* = l^2 N_0 + \frac{l^4}{2}\frac{E_c A_c}{L_0}\int_0^L \left(-\varphi'(s)\right)^2 ds\,. \tag{2.27}$$

To be noticed is that the intrinsic length scale l affects both the local and the nonlocal stiffness, but with different powers. The term $l^2 N_0$ determines the tangent stiffness at the origin. When the tendon is highly pre-stressed with respect to its axial stiffness ($N_0 \gg E_c A_c L/L_0$) and/or the curvature is small ($\varphi'(s) \ll 1/L$), the model falls within the framework of Euler's (local) elastica. In the simplest case of pure bending accoding to an arc of a circle, the rotation field is given by (2.19). Setting ${\varphi_0}^* = \varphi^*(0) = -\varphi^*(L)$, one finds that $(\varphi^*(s))' = -2{\varphi_0}^*/L$, so that the radius of curvature is $\rho = 0.5L/{\varphi_0}^*$. Consequently, assuming for simplicity that $L_0 \simeq L$, equation (2.27) can be written in the form

$$K^* = l^2\left(N_0 + \frac{l^2}{2\rho^2}E_c A_c\right)\,. \tag{2.28}$$

As an order of magnitude $N_0 \simeq 10^{-4} A_c E_c$. Hence, the nonlocal term becomes greater than the local one when approximately $\rho < 70\,l$. This simple example highlights that there is a close correlation between macroscopic curvature and intrinsic length-scale l in the nonlocal term.

2.4. Numerical solutions

The semi-analytical method described in Section 2.3 makes it possible to establish a correspondence between the classical Euler's elastica and its nonlocal counterpart. However, it is much faster nowadays to directly solve numerically the integro-differential equations (2.6-2.7). The comparison of the solutions obtainable with the semi-analytical and the numerical methods

mutually proves their reliability, since the approaches are completely different in type.

The discretized version of the governing equations can be obtained through the approximation (2.14). The interval $[0, L]$ is divided into n equal segments of length $\Delta L = L/n$, and the nonlinear system of algebraic equations (2.15) is solved. Recall that such system corresponds to the solution of flexural tensegrity physical model represented in Figure 2, when the length of the segments coincides with the discretization step. Segmental beams composed of a limited number of segments (of the order of 10) have been analyzed in detail by Boni et al. (2020), but our interest here is to tackle to continuum problem by means of its discrete approximation. Therefore, it is necessary to check the convergence of the numerical solution as the number of subdivisions increases.

For the discretized problem, we have used the numerical solver `fsolve` implemented in Matlab (MathWorks, 2020), which is based on the Levenberg-Marquardt (Moré, 1978) and trust-region (Conn et al., 2000) methods developed from nonlinear least-squares algorithms.

For the rod of Figure 4(a) under a concentrated force $P = 30\,\mathrm{N}$ at midspan, with reference to the case $L = 3\,\mathrm{m}$, $K_L = 10\,\mathrm{Nm}^2$, $K_{NL} = 150\,\mathrm{Nm}^2$ and $l^2 = 0.1\,\mathrm{m}^2$, Figure 5(a) shows the plots of the deformation as the number n of subdivisions is augmented. Figure 5(b) reports the maximum deflection again as a function n. A good approximation is obtained with $n = 49$ since the difference is less than 0.032% when passing to $n = 99$.

It should also be mentioned that fairly accurate estimates of the solution can be obtained by using appropriate shape functions for the rotation field $\varphi(s)$. In particular, consider

$$\varphi(s) = \varphi_0 \cos\left(\frac{\pi s}{L}\right), \tag{2.29}$$

where φ_0 is the shape parameter, representing the rotation at the ends of the simply supported rod (Figure 1). The constraint equation $(2.6)_2$ is automatically satisfied. Then, the shape function is inserted in the energy functional represented by (2.1) and (2.2), which thus becomes an algebraic function of φ_0. The optimal value of φ_0 is found through minimization. A further useful simplification consists in expanding in Taylor's series the sine (up to the fifth order) and cosine functions (up to the fourth order), so that the energy reduces to a polynomial of the 5^{th} degree in φ_0. We have verified that when the midspan deflection is less than $L/5$, this method provides excellent

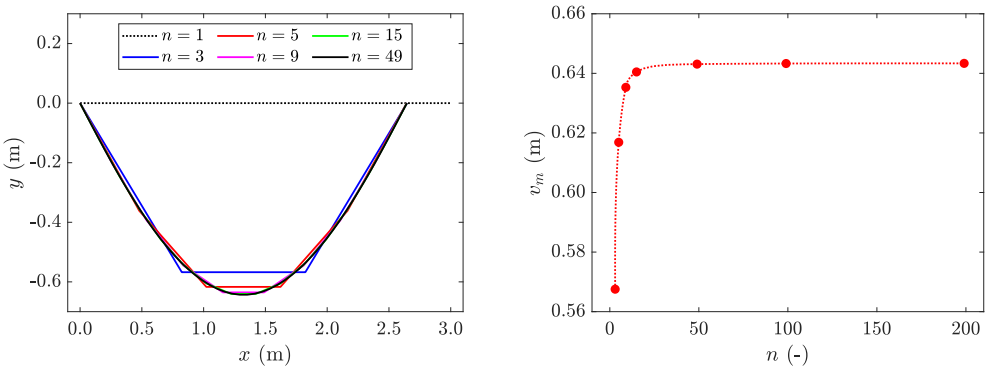

(a) (b)

Figure 5: Numerical results obtained with an increasing number n of subdivisions for a simply supported rod under a concentrated load $P = 30\,\mathrm{N}$ at midspan: (a) Deformed curve for various n and (b) maximum midspan deflection v_m as a function of n. Case $L = 3\,\mathrm{m}$, $K_L = 10\,\mathrm{Nm}^2$, $K_{NL} = 150\,\mathrm{Nm}^2$ and $l^2 = 0.1\,\mathrm{m}^2$.

results under uniformly distributed load, but it is also sufficiently accurate under concentrated load at midspan and for the first mode of axial buckling, as it will be shown in the forthcoming examples.

3. Examples

The rod of Figure 1 is here analyzed when subjected to axial load, concentrated load at midspan and uniformly distributed load. Results obtained with the semi-analytical method illustrated in Section 2.3 are compared with those obtainable with a direct numerical approach, as per Section 2.4. For the case of moderately inflexed rods, with no loops, we discuss the approximation *via* shape function. Unless stated otherwise, reference is made to the case $L = 3\,\mathrm{m}$, $K_L = 10\,\mathrm{Nm}^2$, $K_{NL} = 150\,\mathrm{Nm}^2$ and $l^2 = 0.1\,\mathrm{m}^2$.

3.1. Axial load and buckling

Suppose that only a compression force F is applied ($M_l = M_r = 0$ and $p(s) = 0$). The Lagrange multiplier λ is null and the differential equation (2.6) becomes

$$\left[K_L + K_{NL}\frac{l^2}{L}\int_0^L (\varphi'(s))^2 ds\right]\varphi''(s) + F\sin(\varphi(s)) = 0\,. \tag{3.1}$$

To determine the bifurcation limit for buckling, only small perturbations in a neighborhood of the reference straight configuration need to be considered. Assuming $\varphi \ll 1$, the nonlocal term becomes negligible; setting $\sin(\varphi(s)) \simeq \varphi(s)$, the critical load $F_{cr} = K_L\pi^2/L^2$ is found. For the case at hand $F_{cr} \simeq 10.97\,\mathrm{N}$.

The post-critical deformation (first mode) has been evaluated in three different ways: with the semi-analytical approach, numerically and by using the shape function (2.29). In the latter case, the equilibrium condition furnishes the shape parameter φ_0 as the solution of the equation

$$\left(\frac{K_{NL}l^2\pi^4}{2L^4} + \frac{F}{8}\right)\varphi_0^2 + \left(\frac{K_L\pi^2}{L^2} - F\right) = 0\,. \tag{3.2}$$

Figure 6(a) shows the deformation corresponding to four different values of $F > F_{cr}$. The curves associated with the two lower loads ($F = 20,\ 40\,\mathrm{N}$), calculated with all the three aforementioned methods (semi-analytical, numerical, shape-function), show an excellent correspondence. The other curves ($F = 60,\ 80\,\mathrm{N}$) cannot be accurately determined with the shape function. A quantitative comparison is made in Table 1 in terms of maximum inflexion $|v_m|$ at midspan.

Table 1: Maximum inflexion $|v_m|$ at midspan under the axial load $F > F_{cr}$. Results obtained with the semi-analytical approach, the numerical method and the shape function, and corresponding difference (in percentage) with respect to the semi-analytical solution.

Axial Load F	Semi-analytical	Numerical ($n = 199$)	Percentage difference	Shape function	Percentage difference
20 N	0.7800 m	0.7781 m	0.24 %	0.7742 m	0.74 %
40 N	1.1017 m	1.0997 m	0.18 %	1.0831 m	1.69 %
80 N	1.2097 m	1.2087 m	0.08 %	-	-
380 N	0.9453 m	0.9474 m	0.22 %	-	-

The plot of F against v_m is shown in Figure 6(b), together with the graph corresponding to the case $K_{NL} = 0$, from now on referred to as *Euler's elastica* or *local elastica*. It is clear that the nonlocal term provides additional stiffness since a slight increase of $|v_m|$ with respect to the bifurcation point is associated with an almost quadratic increment of F; on the other hand, in the Euler's elastica, F remains almost constant within the range $|v_m| \leq 0.5\,\mathrm{m}$.

Figure 6(c) reports the bending stiffness K^* as per (2.16) as a function of $|v_m|$. Observe that for large deflections the contribution from the nonlocal

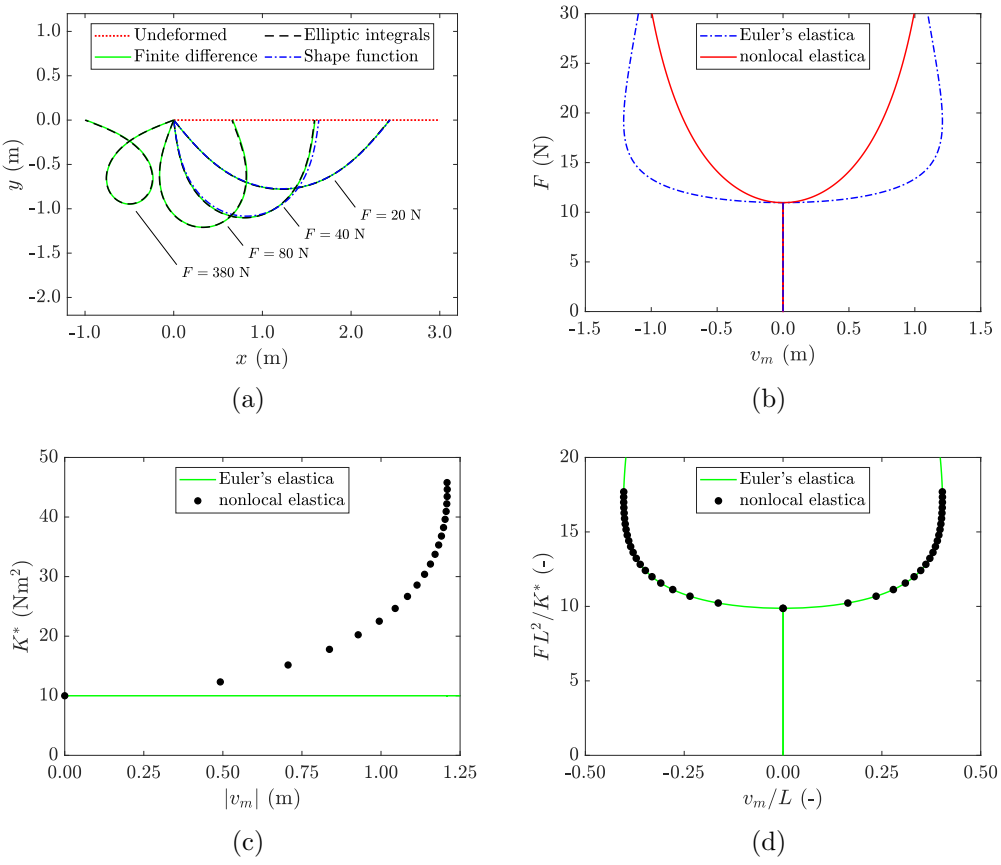

Figure 6: Nonlocal elastica under the axial load $F \geq F_{cr}$. (a) Post-buckling deformation for different values of F; (b) graph of F as a function of the inflexion v_m at midspan and comparison with Euler's elastica; (c) effective stiffness K^* as a function of $|v_m|$; (d) non-dimensional plot of the load-displacement curves.

term may overcome several times the tangent stiffness, which coincides with the stiffness of Euler's elastica.

Figure 6(d) is the most interesting one since it shows the non-dimensional quantity FL^2/K^*, plotted as a function of v_m/L. While presenting the semi-analytical method in Section 2.3, it has been demonstrated that a nonlocal elastica responds as an Euler's elastica with bending stiffness K^* given by (2.16). This means that the deformed shape of Euler's elastica, with bending stiffness K_L, under the force F, perfectly overlaps with the curve attained by the nonlocal elastica when bent by the generic force $F\,K^*/K_L$. Hence, it is not surprising that the black dots, associated with the *nonlocal* model, perfectly overlap with the curve corresponding to the *local* case. In other words, the ratio F/K^* represents the invariant describing the self-similarity associated with the same deformed shape for the local and the nonlocal cases.

For the sake of comparison with a physical model, consider now the flexural tensegrity segmental beam that was illustrated in Figure 3, for which $L = 553.6\,\mathrm{mm}$, $l^2 = 100.6\,\mathrm{mm}^2$, $K_L = 3475\,\mathrm{Nmm}^2$ and $K_{NL} = 21375\,\mathrm{Nmm}^2$. The deformed shapes consequent to the application of the two forces F can be equivalently obtained by imposing the relative displacement of the ends, so that F represents the constraint reaction. Figure 7 reports four different configurations which correspond to the cases illustrated in Figure 6(a) with respect to the aforementioned self-similarity. The blue dots that are overdrawn on the photographs indicate the deformation predicted by the theoretical continuum model with the same material parameters, calculated by using the semi-analytical method. The comparison shows a very good agreement.

3.2. Rod bent by a concentrated force at midspan

When only a concentrated force P acts a midspan ($F = 0$ and $M_l = M_r = 0$), the Lagrange multiplier is $\lambda = P/2$ and the differential equation (2.6) becomes

$$\left[K_L + K_{NL}\frac{l^2}{L}\int_0^L (\varphi'(s))^2 ds\right]\varphi''(s) \pm \frac{P}{2}\cos(\varphi(s)) = 0\,, \tag{3.3}$$

where the "plus" ("minus") sign holds for $L/2 \le s \le L$ ($0 \le s < L/2$).

Using the shape function (2.29) and expanding in Taylor's series the trigonometric functions, as indicated in Section 2.4, one obtains the polynomial equation

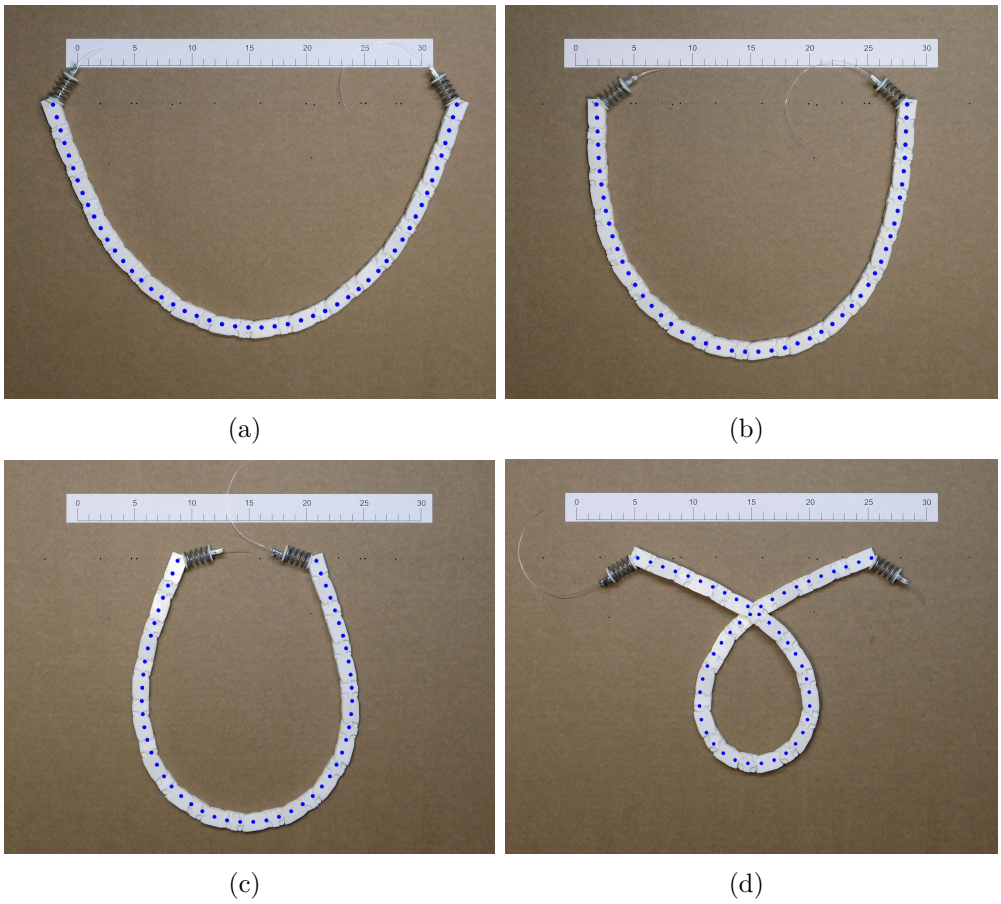

Figure 7: Post-buckling deformations of the flexural tensegrity segmental beam for different values of the relative displacement assigned at the ends. Imposed end displacements correspond to axial force: (a) $u(L) = 198\,\mathrm{mm}$, (b) $u(L) = 286\,\mathrm{mm}$, (c) $u(L) = 432\,\mathrm{mm}$ and (d) $u(L) = 755\,\mathrm{mm}$ (closed loop). The overdrawn blue dots correspond to the semi-analytical solution of the nonlocal-elastica continuum model.

Table 2: Maximum inflexion v_m under concentrated load P at midspan. Results obtained with the semi-analytical approach, the numerical method and the shape function, and corresponding difference (in percentage) with respect to the semi-analytical solution.

midspan Load P	Semi-analytical	Numerical ($n = 199$)	Percentage difference	Shape function	Percentage difference
20 N	0.6448 m	0.6434 m	0.22 %	0.6314 m	2.08 %
80 N	1.0085 m	1.0068 m	0.17 %	0.9734 m	3.48 %
160 N	1.1340 m	1.1325 m	0.13 %	-	-

$$P\,\frac{1}{45}\,\frac{L}{\pi}\,\varphi_0^4 - \frac{K_{NL}l^2\pi^4}{4L^3}\,\varphi_0^3 - P\,\frac{1}{3}\,\frac{L}{\pi}\,\varphi_0^2 - \frac{K_L\pi^2}{2L}\,\varphi_0 + P\,\frac{L}{\pi} = 0\,. \tag{3.4}$$

The plots of the deformed shape obtained with the semi-analytical method, the numerical approach and the shape function are juxtaposed in Figure 8(a). The agreement between the semi-analytical and numerical methods is again excellent. The accuracy of the shape function is still rather good, with maximum differences in terms of v_m of about 3.5%, at least for the loads $P = 20,\, 80\,N$ (the case $P = 160\,\mathrm{N}$ is not considered because accuracy is lost). The quantitative comparison in terms of maximum deflection v_m is recorded in Table 2, which is the counterpart of Table 1.

The relationships between P and v_m are plotted in Figure 8(b) and compared with the local model of Euler's elastica: the additional stiffness provided by the nonlocal term is evident. Figure 8(c) reports the effective stiffness K^* for increasing inflexion, measured through the variable v_m. Figure 8(d), which is the counterpart of Figure 6(d), shows the non-dimensional plot of the load-displacement curves for Euler's elastica and the nonlocal elastica. Again the black dots, corresponding to the nonlocal case, perfectly overlap with the graph corresponding to local case. This confirms what already indicated for case of the axial force: the nonlocal elastica is equivalent to a local Euler's elastica with a bending stiffness that depends upon the deformation.

Figure 9 reports the comparison between the response of the flexural tensegrity segmental beam of Figure 3, with the same constitutive parameters, and that of the nonlocal model (blue dots). The effect of a concentrated load at midspan has been equivalently evaluated by imposing a vertical displacement at the same point. The agreement is again very good.

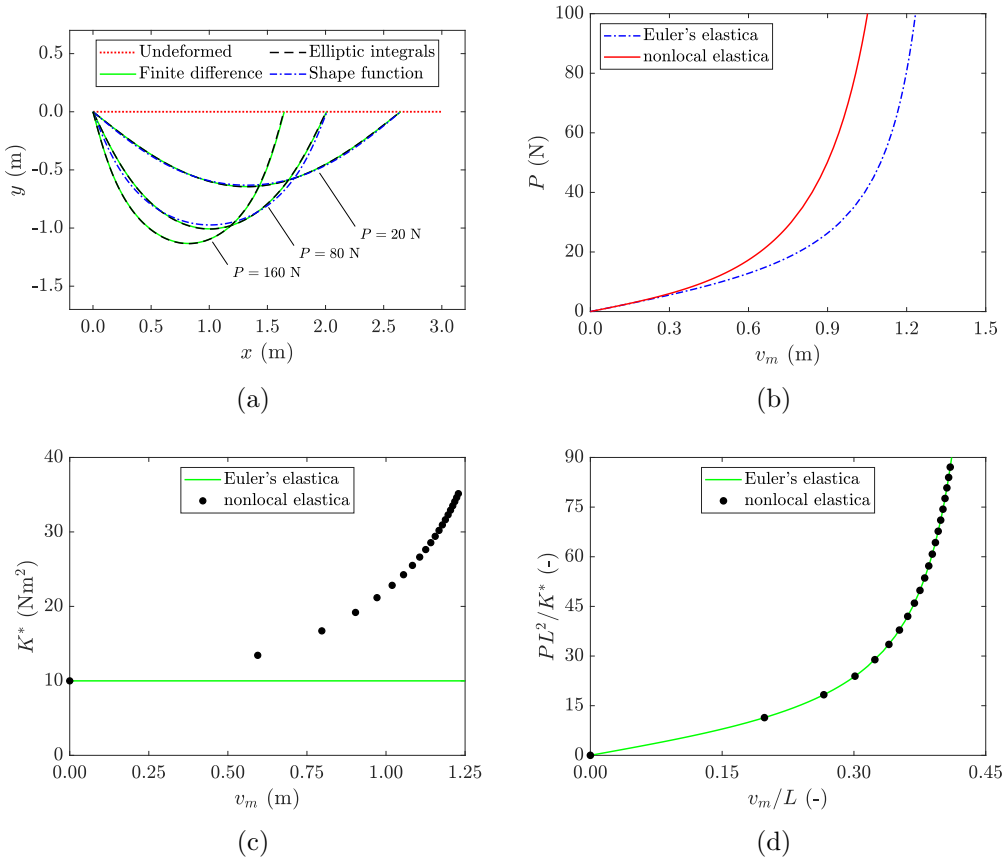

Figure 8: Nonlocal elastica under the concentrated load P at midspan. (a) Deformation for different values of P; (b) graph of P as a function of maximum inflexion v_m at midspan and comparison with Euler's elastica; (c) effective stiffness K^* as a function of v_m; (d) non-dimensional plot of the load-displacement curves.

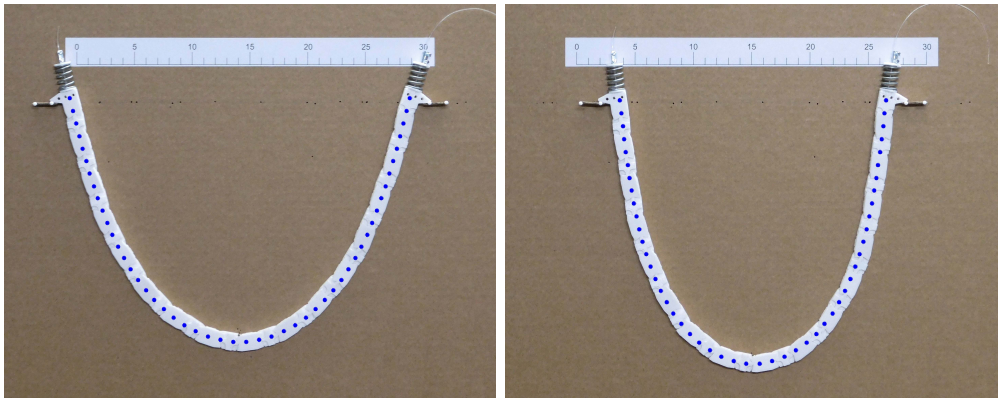

(a) (b)

Figure 9: Flexural tensegrity segmental beam under imposed displacements at midspan (equivalent to concentrated load at midspan): (a) $v(L/2) = 211\,\text{mm}$ and (b) $v(L/2) = 226\,\text{mm}$. The overdrawn blue dots correspond to the semi-analytical solution of the nonlocal-elastica continuum model.

3.3. Rod bent by uniformly distributed load per unit length

Having set $M_l = M_r = 0$ and $F = 0$, the effect of a uniformly distributed load $p(s) = p_0$ is now investigated. The solution has been obtained either by means of the shape function (2.29) or numerically. For this case, the semi-analytical method is not feasible. An analytical solution for Euler's elastica has been presented by Mingari Scarpello and Ritelli (2011) in terms of Lauricella's hypergeometric functions, but it is limited to the range $0.0594 < p_0 L^3/K^* < 6$ and its expression is really complicated.

For this case, the Lagrange multiplies is $\lambda = p_0 L/2$ and the differential equation (2.6) becomes

$$\left[K_L + K_{NL}\frac{l^2}{L}\int_0^L (\varphi'(s))^2 ds\right]\varphi''(s) + p_0\,\frac{L-2s}{2}\,\cos(\varphi(s)) = 0\,. \qquad (3.5)$$

By using the shape function (2.29) and expanding in Taylor's series the trigonometric functions, one obtains the polynomial equation

$$p_0\,\frac{149}{2700}\,\frac{L^2}{\pi^2}\,\varphi_0^4 - \frac{K_{NL}l^2\pi^4}{4L^3}\,\varphi_0^3 - p_0\,\frac{7}{9}\,\frac{L^2}{\pi^2}\,\varphi_0^2 - \frac{N_0 l^2\pi^2}{2L}\,\varphi_0 + 2\,p_0\,\frac{L^2}{\pi^2} = 0\,. \quad (3.6)$$

The deformations resulting from the two approaches (numerical and shape function) are juxtaposed in Figure 10(a) for $p_0 = 10, 30, 100\,\mathrm{N/m}$. Table 3 records the maximum deflection v_m as a function of p_0. Observe that the shape function provides a difference less than 0.5% with respect to the numerical calculation when $v_m < L/3$.

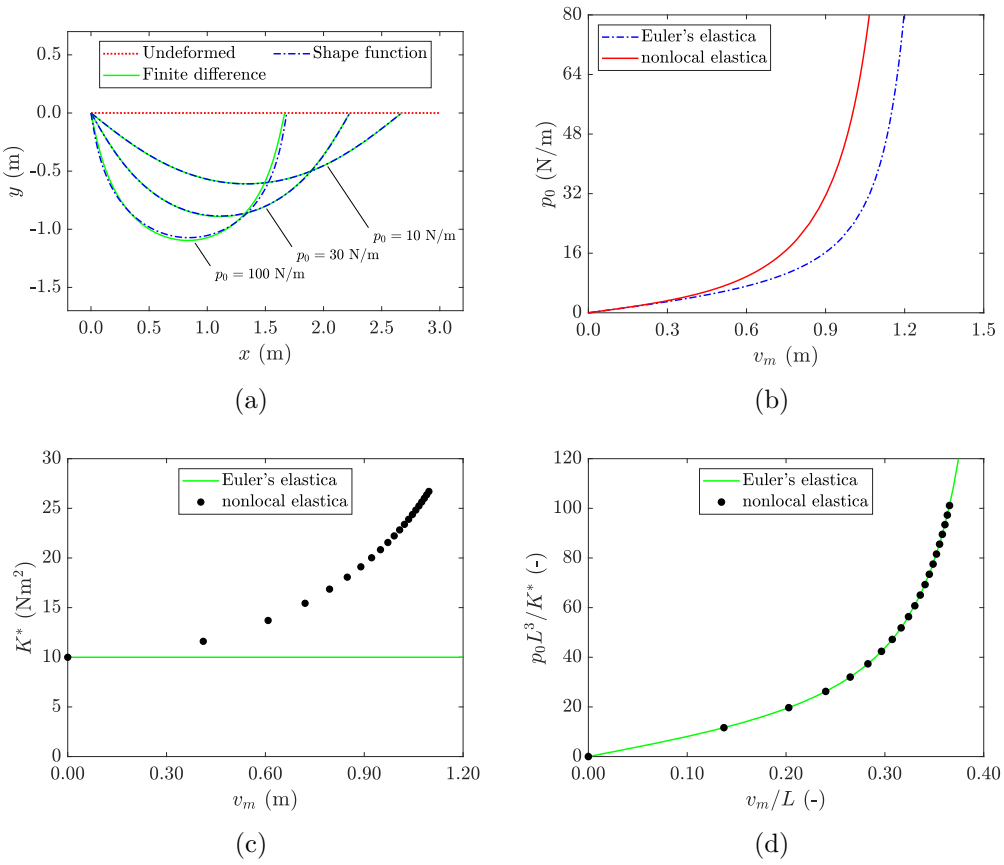

Figure 10: Nonlocal elastica under uniformly distributed load p_0. (a) Deformation for different values of p_0; (b) graph of p_0 as a function of maximum inflexion v_m at midspan and comparison with Euler's elastica; (c) effective stiffness K^* as a function of v_m; (d) non-dimensional plot of the load-displacement curves.

The dependence of v_m on p_0 is shown in Figure 10(b). Figure 10(c) compares the values of K^* against v_m for the nonlocal case (black dots) and the local Euler's elastica (continous line). The same conclusions drawn in the

Table 3: Maximum inflexion v_m under uniformly distributed load p_0. Results obtained numerically and with the shape function, and corresponding difference (in percentage).

Distributed Load p_0	Numerical ($n = 199$)	Shape function	Percentage error
10 N/m	0.6082 m	0.6097 m	0.25 %
30 N/m	0.8897 m	0.8861 m	0.40 %
100 N/m	1.0962 m	1.0719 m	2.22 %

previous Sections 3.1 and 3.2 also apply in this case. The non-dimensional plot of the function $p_0 L^3/K^*$ vs. v_m/L, shown in Figure 10(d), confirms again that the nonlocal elastica perfectly corresponds to an equivalent Euler's elastica with appropriate stiffness.

Figure 11 shows the comparison between the deformation of nonlocal elastica (blue dots), numerically calculated, and the flexural tensegrity beam under uniformly distributed loads corresponding to the self-weight. The two different deflections have been obtained by varying the initial tensile force in the cable (either $N_0 = 23.7\,\mathrm{N}$ or $N_0 = 44.1\,\mathrm{N}$), which is equivalent to a variation in the initial stiffness, so that, for the tested model, one has $L = 553.6\,\mathrm{mm}$, $l^2 = 100.6\,\mathrm{mm}^2$, either $K_L = 2383\,\mathrm{Nmm}^2$ or $4435\,\mathrm{Nmm}^2$, and $K_{NL} = 21375\,\mathrm{Nmm}^2$. Again the theoretical and the physical models provide overlapping results.

3.4. An application to the bow

As a further illustrative example, the nonlocal elastica is now applied to form the limbs of a new type of bow. The theoretical problem of the bow has been considered by a number of authors, who generally use the classical model of the elastica to determine the bow efficiency (Kooi and Sparenberg, 1980). The following analysis is based on the following simplifying hypotheses: i) the upper and the lower limbs form a continuous beam; ii) the bowstring is inextensible; iii) the bow inertia is disregarded. Figure 12 shows a scheme of the bow in the reference configuration after stringing and while nocking the arrow. The structural parameters for this case are $K_L = 20.0\,\mathrm{Nm}^2$ and $K_{NL} = 112.5\,\mathrm{Nm}^2$. The total length of the beam formed by the two limbs, supposed straight in the unstrained reference configuration before the stringing process, is $L = 150\,\mathrm{cm}$. Assuming that the bowstring length is equal to $L_s = 146.2\,\mathrm{cm}$, after stringing, the arch formed by the beam has a sag $f_0 = 15\,\mathrm{cm}$.

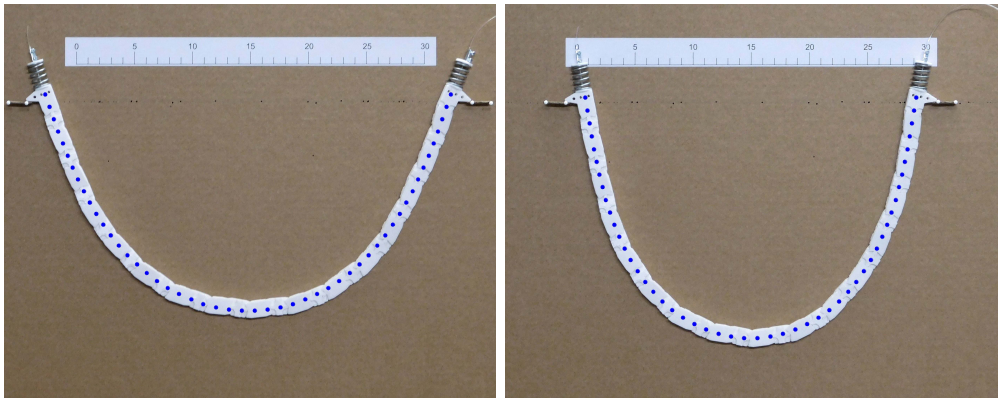

(a) (b)

Figure 11: Flexural tensegrity segmental beam under uniformly distributed load. The distributed load was self-weight ($P_i = 0.02\,\mathrm{N}$ for each segment i, $i = 1 \ldots 32$) and the different value of deflection is obtained by varying the tension force in the cable: (a) $N_0 = 44.1\,\mathrm{N}$ and (b) $N_0 = 23.7\,\mathrm{N}$. The overdrawn blue dots correspond to the semi-analytical solution of the nonlocal-elastica continuum model.

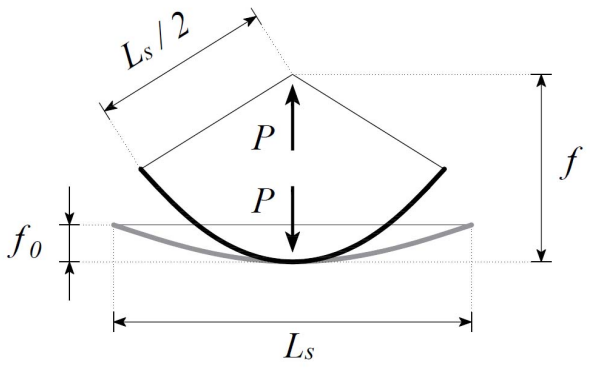

Figure 12: Schematic representation of the bow in the reference configuration after stringing (grey line) and while nocking the arrow (black color).

When the arrow is fired, the problem is equivalent to that in which a mass m (the arrow) is accelerated by the elastic return of the bow. The force P transmitted to the arrow is a function of sag f, which are both function of the time t. Setting $P = P(f)$ or, equivalently, $P = P\left(f(t)\right) = \hat{P}(t)$, the governing equations are $m\ddot{f}(t) = -\hat{P}(t)$, with initial conditions $f(0) = \bar{f}$ and $\dot{f}(0) = 0$, where $\bar{f}$ is the maximum elongation of the bow. The arrow is released when $f = f_0$ and $P(f_0) = 0$.

Figure 13(a) reports the plot of the function $P = P(f)$ for the considered nonlocal elastica and, for the sake of comparison, for a classical Euler's elastica whose (constant) bending stiffness is equal to the mean value of the effective stiffness K^* for the nonlocal case in a reasonable range for the parameter f. In particular, Figure 13(b) shows the stiffness K^* of (2.27) as a function of f and the stiffness of the Euler's elastica in the comparison. Figures 13(c) and 13(d) indicate the plots of $f = f(t)$ and $P = \hat{P}(t)$, respectively, for an arrow with mass $m = 0.02\,\mathrm{kg}$. Here, two curves are reported for the Euler's elastica, which correspond either to the case of equal maximum elongation $\bar{f} = 72.7\,\mathrm{cm}$, or to equal maximum force $\bar{P} = 110.8\,\mathrm{N}$, with respect to the nonlocal case. Obviously, for the same $\bar{f}$, the force $P(\bar{f})$ is lower in Euler's elastica; keeping fixed $\bar{P}$, the bow made with Euler's elastica shall be stretched more.

When the maximum elongation $\bar{f}$ is set equal to $72.7\,\mathrm{cm}$, the nonlocal bow requires $26.5\,\mathrm{J}$ for nocking, while the classical bow needs $25.4\,\mathrm{J}$ (about 4% less), and, consequently, the top speed, neglecting all possible sources of dissipations, is respectively equal to $51.5\,\mathrm{m/s}$ and $50.4\,\mathrm{m/s}$. On the other hand, when the maximum force $\bar{P}$ is $110.8\,\mathrm{N}$, the classical bow excels in top speed ($60.4\,\mathrm{m/s}$) as the elongation is much larger, but it requires much more energy ($36.5\,\mathrm{J}$). In any case, apart from the specific result, this elementary example highlights the effect of the nonlocal constitutive properties.

This simple example illustrates one possible application of the nonlocal elastica, but a detailed study of the optimal design for a bow certainly deserves further work. The major advantage of the flexural tensegrity concept is that a tailored response can be obtained by simply varying the shape of the pitch lines for the contact surfaces of adjacent segments. A very effective design could be achieved by shaping the pitch lines in such a way as to obtain a sublinear moment-curvature relationship. In fact, the force exerted by the archer should be minimal when the arrow is just about to be shot (maximum bow draw), because in this case it is easier to aim. In traditional bows, this condition is pursued by appropriately shaping the limbs, or by introducing

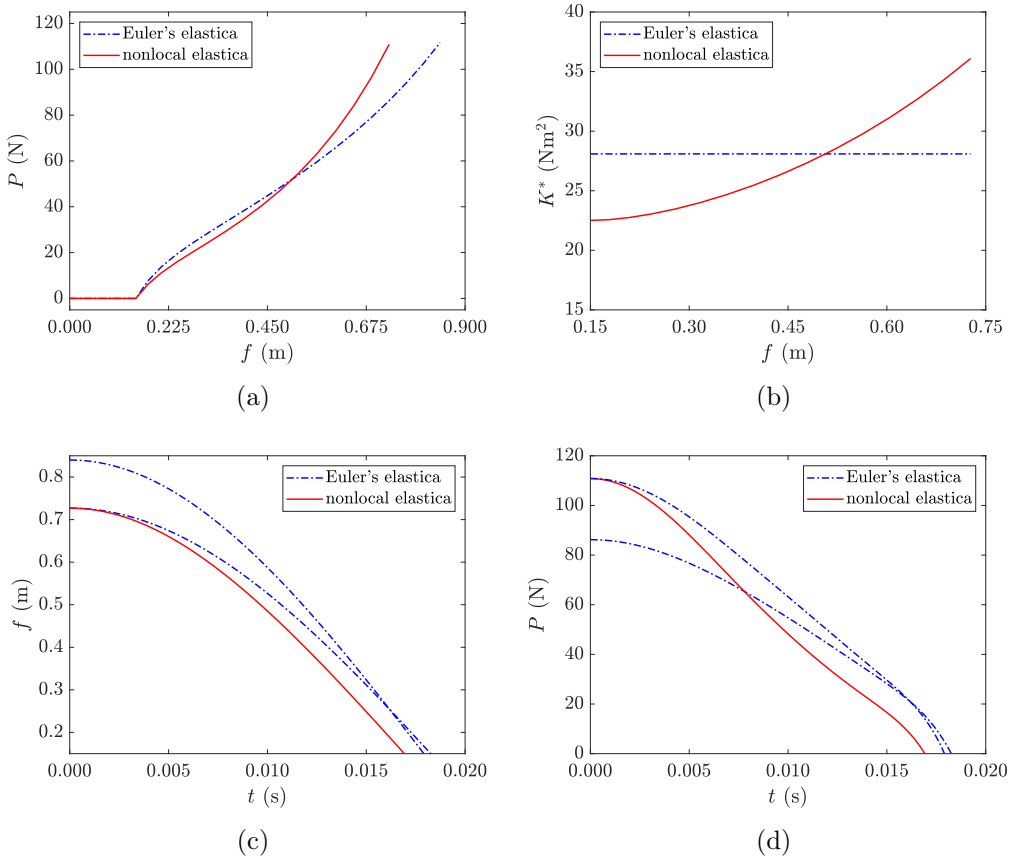

Figure 13: Response of the bow when the arrow is fired. (a) Force P, due to the elastic return of the bow, as a function of the bow elongation f; (b) effective stiffness K^* as a function of f; (c) Dependence of f on time t for the nonlocal and the classical Euler's model (two curves corresponding to either equal maximum elongation or equal maximum force); (d) Corresponding dependence of P on time t.

additional pulleys between the limbs and the bowstring (modern compound bow). In flexural-tensegrity bows, this could be directly achieved by appropriately shaping the pitch lines of the segments in contact. Of course, the theoretical design should be validated by manufacturing a prototype, but this goes beyond the scope of the present article, where we have limited ourselves to considering the simplest case in which the level arm $a(s)$, introduced in Section 2.2, is a linear function of the curvature.

4. Conclusions

A particular model has been proposed, suitable for representing an inflexed lamina that responds to applied loads as an Euler's elastica, but its flexural stiffness, while remaining homogeneously constant along the whole structure, depends on the entire curvature field according to an integral average. For this reason, the theory falls into the category of nonlocal models, recovering the classical Euler's description when the nonlocal term in the constitutive relation is negligible. The proposed theory does not carry the inconsistencies, especially for what regards the edge conditions, of other nonlocal models for beams, in which the bending depends on the convolution of the curvature field with an averaging kernel, with compact support or fast decay at infinity. The analytical research of the equilibrium configurations of the nonlocal elastica under imposed loads borrows the same methods as the classic Euler's elastica, implying the solution of elliptic integrals and the use of hypergeometric functions. This type of approach has been confirmed by a direct numerical calculation in exemplificatory model problems, for which the possibility of using shape functions to approximate moderate curvature fields has also been investigated.

The motivation stems from the concept of flexural tensegrity, already presented for the discrete case, according to which the flexural integrity of segments in unilateral contact, with properly profiled contact surfaces, is made possible by prestressing tendons that press the segments together, so to provide a certain stiffness against bending. The discretization of the equilibrium equations of the continuum model not only represents the basis for their numerical solution, but also corresponds to the equilibrium of a flexural tensegrity segmental beam, formed by segments of length equal to the discretization step. The so-established correspondence between the continuum theory and the discrete physical model provides an intuitive interpretation of the material parameters that regulate the response of the nonlocal elastica,

since they can be related to the mechanical properties of the tendon and the design profile of the contact surfaces between the segments.

On the one hand, the proposed theory can serve as a continuous approximation of the discrete case of flexural tensegrity segmental beams; on the other hand, it can constitute an autonomous model per se, to describe the behavior of complex one-dimensional structures beyond the classic Euler's model. Potential fields of application are both in medicine and engineering, to manufacture elements whose shape or rigidity can be adjusted and adapted to specific service needs, such as micro-devices for surgery, robotic components, aerospace structures with active control of vibrations. The movement of the limbs of microorganisms, such as the flagella of bacteria, or the mechanical characteristics of macromolecules, such as nucleic acids, could be interpreted by the flexural properties of the nonlocal elastica, especially in their capability of being transformed with very small variations at the level of the underlying microstructural constituents. Possible applications are yet to be fully explored and appreciated.

Data accessibility. This article has no additional data.

Authors' contribution. The authors jointly developed the theoretical model, wrote the paper and gave final approval for publication.

Competing interests. There are no competing interests to declare.

Funding. This research has not been supported by any specific grant from funding agencies in the public, commercial, or not-for-profit sectors.

References

Armanini, C., Dal Corso, F., Misseroni, D., Bigoni, D., 2017. From the elastica compass to the elastica catapult: an essay on the mechanics of soft robot arm. Proceedings of the Royal Society A: Mathematical, Physical and Engineering Sciences 473, 20160870. doi:10.1098/rspa.2016.0870.

Armanini, C., Dal Corso, F., Misseroni, D., Bigoni, D., 2019. Configurational forces and nonlinear structural dynamics. Journal of the Mechanics and Physics of Solids 130, 82–100. doi:10.1016/j.jmps.2019.05.009.

Beatini, V., Royer-Carfagni, G., 2013. Cable-stiffened foldable elastica for movable structures. Engineering Structures 56, 126–136. doi:10.1016/j.engstruct.2013.02.009.

Bigoni, D., 2012. Nonlinear solid mechanics: bifurcation theory and material instability. 1 ed., Cambridge University Press, Cambridge, UK. doi:10.1017/CBO9781139178938.

Bisshopp, K., Drucker, D., 1945. Large deflection of cantilever beams. Quarterly of Applied Mathematics 3, 272–275. doi:10.1090/qam/13360.

Boni, C., Silvestri, M., Royer-Carfagni, G., 2020. Flexural tensegrity of segmental beams. Proceedings of the Royal Society A: Mathematical, Physical and Engineering Sciences 476, 20200062. doi:10.1098/rspa.2020.0062.

Bosi, F., Misseroni, D., Dal Corso, F., Bigoni, D., 2014. An elastica arm scale. Proceedings of the Royal Society A: Mathematical, Physical and Engineering Sciences 470, 20140232. doi:10.1098/rspa.2014.0232.

Bosi, F., Misseroni, D., Dal Corso, F., Bigoni, D., 2015a. Development of configurational forces during the injection of an elastic rod. Extreme Mechanics Letters 4, 83–88. doi:10.1016/j.eml.2015.04.007.

Bosi, F., Misseroni, D., Dal Corso, F., Bigoni, D., 2015b. Self-encapsulation, or the 'dripping' of an elastic rod. Proceedings of the Royal Society A: Mathematical, Physical and Engineering Sciences 471, 20150195. doi:10.1098/rspa.2015.0195.

Brun, P.T., Ribe, N., Audoly, B., 2014. An introduction to the mechanics of the lasso. Proceedings of the Royal Society A: Mathematical, Physical and Engineering Sciences 470, 20140512. doi:10.1098/rspa.2014.0512.

Chen, J., Li, C., 2007. Planar elastica inside a curved tube with clearance. International journal of solids and structures 44, 6173–6186. doi:10.1016/j.ijsolstr.2007.02.021.

Conn, A., Gould, N., Toint, P., 2000. Trust region methods. volume 1. Siam, Philadelphia, USA. doi:10.1137/1.9780898719857.

Diamant, J., Keller, A., Baer, E., Litt, M., Arridge, R., 1972. Collagen; ultrastructure and its relation to mechanical properties as a function of ageing. Proceedings of the Royal Society of London B: Biological Sciences 180, 293–315. doi:10.1098/rspb.1972.0019.

Eringen, A., 1983. On differential equations of nonlocal elasticity and solutions of screw dislocation and surface waves. Journal of Applied Physics 54, 4703–4710. doi:10.1063/1.332803.

Euler, L., 1744. Methodus Inveniendi Lineas Curvas Maximi Minimive Proprietate Gaudentes sive Solutio Problematis Isoperimetrici Latissimo Sensu Accepti. volume 1. M.-M. Bosquet & Socios, Lausanne & Geneve.

Euler, L., 1952. Methodus Inveniendi Lineas Curvas Maximi Minimive Proprietate Gaudentes, sive Solutio Problematis Isoperimetrici Lattissimo Sensu Accepti: Additamentum 1 De Curvis Elasticis. Leonhardi Euleri Opera Omnia, Series prima (Opera mathematica), Vol. XXIV, Auctoritate et impensis Societatis Scientiarum Naturalium Helveticae, Orell Füssli, Zürich.

Fosdick, R., James, R., 1981. The elastica and the problem of the pure bending for a non-convex stored energy function. Journal of Elasticity 11, 165–186. doi:10.1007/BF00043858.

Froli, M., Royer-Carfagni, G., 2000. A mechanical model for the elastic-plastic behavior of metallic bars. International Journal of Solids and Structures 37, 3901–3918. doi:10.1016/S0020-7683(99)00069-4.

Jahnke, E., Emde, F., 1945. Tables of functions with formulae and curves. 4 ed., Dover Publications, New York, USA.

Kooi, B., Sparenberg, J., 1980. On the static deformation of a bow. Journal of engineering mathematics 14, 27–45. doi:10.1007/BF00042863.

Lauricella, G., 1893. Sulle funzioni ipergeometriche a piu variabili. Rendiconti del Circolo Matematico di Palermo 7, 111–158. doi:10.1007/BF03012437.

Love, A., 1944. A Treatise on the Mathematical Theory of Elasticity. 4 ed., Cambridge University Press, Cambridge, UK.

MathWorks, 2020. fsolve. https://it.mathworks.com/help/optim/ug/fsolve.html#butbmfz-5. Accessed: 2020-05-08.

Mingari Scarpello, G., Ritelli, D., 2011. Exact solutions of nonlinear equation of rod deflections involving the lauricella hypergeometric functions. International Journal of Mathematics and Mathematical Sciences 2011. doi:10.1155/2011/838924.

Moré, J., 1978. The levenberg-marquardt algorithm: implementation and theory, in: Numerical analysis. Springer, pp. 105–116. doi:10.1007/BFb0067700.

Newman, B., 1975. Shape of a towed boom of logs. Proceedings of the Royal Society of London. A. Mathematical and Physical Sciences 346, 329–348. doi:10.1098/rspa.1975.0179.

Oldfather, W.A., Ellis, C.A., Brown, D.M., 1933. Leonhard Euler's elastic curves. Isis 20, 72–160. URL: http://www.jstor.org/stable/224885.

Romano, G., Barretta, R., 2017. Nonlocal elasticity in nanobeams: the stress-driven integral model. International Journal of Engineering Science 115, 14–27. doi:10.1016/j.ijengsci.2017.03.002.

Romano, G., Barretta, R., Diaco, M., Marotti de Sciarra, F., 2017. Constitutive boundary conditions and paradoxes in nonlocal elastic nanobeams. International Journal of Mechanical Sciences 121, 151–156. doi:10.1016/j.ijmecsci.2016.10.036.

Royer-Carfagni, G., 2001. Can a moment-curvature relationship describe the flexion of softening beams? European Journal of Mechanics, A/Solids 20, 253–276. doi:10.1016/S0997-7538(00)01128-1.

Royer-Carfagni, G., Buratti, G., 2007. Plastic hinges as phase transitions in strain softening beams. Journal of Mechanics of Materials and Structures 2, 1677–1699. doi:10.2140/jomms.2007.2.1677.

Sadao, S., 1996. Fuller on tensegrity. International Journal of Space Structures 11, 37–42. doi:10.1177/026635119601-206.

Søndergaard, A., Feringa, J., Nørbjerg, T., Steenstrup, K., Brander, D., Graversen, J., Markvorsen, S., Bærentzen, A., Petkov, K., Hattel, J., Knudsen, L., Kortbek, J., 2016. Robotic hot-blade cutting, in: Robotic Fabrication in Architecture, Art and Design 2016. Springer, pp. 150–164. doi:10.1007/978-3-319-26378-6_11.

Thai, H.T., 2012. A nonlocal beam theory for bending, buckling, and vibration of nanobeams. International Journal of Engineering Science 52, 56–64. doi:10.1016/j.ijengsci.2011.11.011.

Thomson, W., Tait, P., 1883. Treatise on natural philosophy. volume 1, part 2. 2 ed., C.J. Clay, M.A. & Son (Cambridge University Press Warehouse), London, UK.

Tournus, M., Kirshtein, A., Berlyand, L., Aranson, I., 2015. Flexibility of bacterial flagella in external shear results in complex swimming trajectories. Journal of the Royal Society Interface 12, 20140904. doi:10.1098/rsif.2014.0904.

Wilson, J., Snyder, J., 1988. The elastica with end-load flip-over. Journal of Applied Mechanics 55, 845–848. doi:10.1115/1.3173731.

Yamada, A., Watari, M., Mochiyama, H., Fujimoto, H., 2007. A jumping robot based on the closed elastica, in: 2007 International Symposium on Micro-NanoMechatronics and Human Science, IEEE. pp. 604–609. doi:10.1109/MHS.2007.4420924.